



The Electric Field outward of Saturn’s Main Rings

C. Paranicas^{1,6} , E. Roussos^{2,6} , K. Dialynas^{3,6} , P. Kollmann¹ , N. Krupp² , M. Hedman⁴ , R. C. Allen¹ , and G. Hospodarsky⁵ 

¹ APL, 11100 Johns Hopkins Rd., Laurel, MD 20723, USA; chris.paranicas@jhuapl.edu

² Max Planck Institute for Solar System Research, Justus-von-Liebig-Weg 3 37081, Goettingen, Germany

³ Office of Space Research and Technology, Academy of Athens, 10679 Athens, Greece

⁴ University of Idaho, ID, USA

⁵ University of Iowa, IA, USA

Received 2022 April 14; revised 2022 May 23; accepted 2022 May 26; published 2022 July 20

Abstract

Cassini data are consistent with a global electric field in Saturn’s magnetosphere that points approximately antisunward. The inner radial extent of this field was initially established using Saturn orbit insertion data but measurements of ultrarelativistic electrons from that pass cast some doubt on whether the electric field reaches all the way to the A ring. It was not until the so-called ring-grazing and proximal orbits near the end of the mission in 2017 that relevant data were again obtained on magnetic field lines that connect to the region just outward of the main rings. Here we report on the energetic charged particle data during those orbits, showing that electron observations at a wide range of energies are consistent with an electric field that influences charged particle drift paths near the outer edge of the A ring. We include a very detailed analysis of Cassini’s ultrarelativistic electron measurements (channel E7 in the text) and argue they provide no information about the electric field. This result further strengthens the case of several studies that have used the presence of the electric field to explain signatures of acceleration in the data.

Unified Astronomy Thesaurus concepts: [Planetary rings \(1254\)](#); [Magnetic fields \(994\)](#)

1. Introduction

The motion of plasma in Saturn’s inner magnetosphere is mainly in the direction of corotation. But some data obtained by the Cassini spacecraft reveal small deviations from this picture that have important implications. Roussos et al. (2010) found that the wakes that formed as a result of the absorption of energetic charged particles by moons did not remain on the same L shell when observed at longitudes far from the satellites that created them. Those and other data, which we describe below, appear to be consistent with a global, nonradial electric field, i.e., a field not associated with the corotating plasma.

The source of this field may be, in part, related to corotating interaction regions (CIRs) in the solar wind. Even deep within the rotationally dominated magnetosphere of Saturn, data have connected energetic electron fluxes to CIRs, down to at least $L = 4$ (Roussos et al. 2014, 2018; Yuan et al. 2020). This was on the basis of quasiperiodic variations in the electron fluxes and in the outer electron radiation belt boundary, with a timescale characteristic of CIR recurrence (~ 2 weeks). Solar wind disturbances can penetrate deeper into magnetospheres if the responding internal pressures are low. Bagenal & Delamere (2011) suggest Jupiter magnetospheric pressures may be > 10 nPa while Saturn’s are < 1 nPa. By comparison, Went et al. (2011), for example, consider solar wind pressures upstream of Saturn that are less than 0.2 nPa. In Saturn’s inner magnetosphere, there are frequent charged–neutral interactions that convert energetic ions to cold ions and this may account for the

generally low plasma pressures found there (see also, Dialynas et al. 2013, 2018). Finally, Jia & Kivelson (2016) proposed an electric field could result from the plasma flow pattern in local time that responds to the distance to the magnetopause in local time. However, such an electric field would be due to a structural situation and, since it is a transient phenomenon, a variable driver would still be required.

A nonrotational electric field at Saturn was originally proposed in Paranicas et al. (2010) to explain measurements made just outward of the A ring. That paper showed data from the Magnetosphere Imaging Instrument (MIMI) obtained during Cassini’s initial passage over the main rings of the planet. They reported that fluxes in some channels of the Low Energy Magnetosphere Measurement System (LEMMS) sensor were not symmetric on magnetic field lines that mapped to the outer edge of the A ring on the dayside and nightside of the planet. Specifically, they found the flux decrease near noon, expected from the absorption at the main ring edge, actually occurred outward of the main rings. They suggested an electric field pointing from noon to midnight could be responsible for creating drift paths that would be consistent with the local time behavior of the flux. Thomsen et al. (2012) republished Cassini waves data from Gurnett et al. (2005) that extracted the electron plasma density near the main rings and confirmed that the drift paths of plasma electrons near Saturn’s main rings showed a similar offset on the dayside only. In this paper, we will be presenting MIMI/LEMMS data from Saturn orbit insertion (SOI), the F-ring or ring-grazing orbits (30 November 2016 to 22 April 2017) and the proximal orbits (22 April 2017 to 15 September 2017).

Initially, Roussos et al. (2005, 2007, 2010) pointed out that satellite microsignatures revealed radial motion in the magnetosphere. The idea was further developed in Andriopoulou et al. (2012, 2014), where they established the statistical, “transient,”

⁶ C. Paranicas, E. Roussos, and K. Dialynas contributed equally to this work.



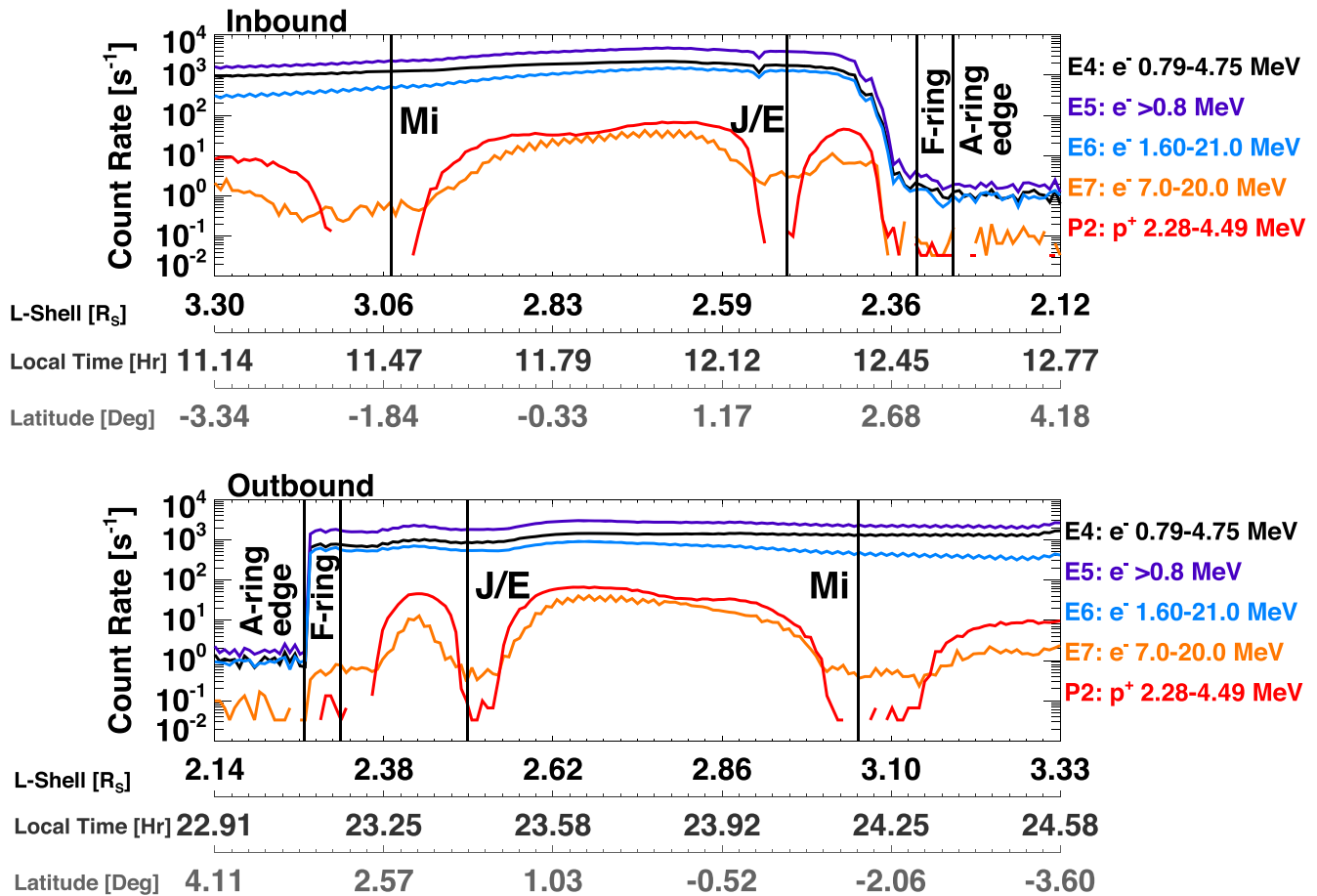


Figure 1. Count rate vs. time for several LEMMS channels around SOI. At the level of a few counts per second or fewer, care must be exercised in interpreting the data.

or nonpermanent nature of the electric field and its global extent. Wilson et al. (2013) further confirmed that the bulk plasma flow vectors were consistent with such a picture. Roussos et al. (2019) went on to analyze energetic electron data from Cassini’s proximal orbits, in the region initially studied by Paranicas et al. (2010) but at higher latitudes, and found further support for an electric field penetrating as deep as the main rings and suggested a CIR-related origin. Specifically, data revealed that the flux dropout on the dayside near the A ring was always radially outward of the ring edge, similar to what SOI data showed, while the magnitude of this offset oscillated with a period of 2 weeks. Roussos et al. (2019) also noted the presence of noncircumplanetary, localized MeV electron enhancements (microbelts), the topology of which appeared to be fully consistent with a noon-to-midnight electric field. Other evidence of the field’s existence is the presence of discrete, accelerated populations, commonly observed in the Cassini data (e.g., Hao et al. 2020).

But the work of Roussos et al. (2019) focused primarily on a single LEMMS electron channel and did not include the LEMMS channel responding to 7–20 MeV electrons (called “E7”), the SOI recordings of which, according to Thomsen et al. (2012), did not seem to be consistent with the picture of a global electric field. In this paper, we will present evidence that the E7 channel cannot be used for the purposes of inferring the electric field near the rings and the proximal orbit data are still consistent with a global electric field extending from the main rings outward.

2. Energetic Electron Orbits close to the Main Rings

In Figure 1, we show LEMMS data obtained during SOI around the beginning of day 2004–183. The following features are notable: energetic electron fluxes measured by channels E4 (0.79–4.75 MeV electrons), E5 (>0.8 MeV electrons), and E6 (1.6–21 MeV electrons) decrease rapidly inbound to Saturn at about $2.4 R_S$, i.e., well outward of the outer edge of the A ring at $2.27 R_S$ ($1 R_S = 60,268$ km; the equatorial radius of Saturn). On the other hand, the fluxes in the same energy channels returned to high levels at the edge of the main rings during the outbound portion of SOI, prior to local midnight. The other two channels shown, E7 (7–20 MeV electrons) and P2 (2.28–4.49 MeV protons, but most likely dominated by higher energy penetrating >60 MeV protons; see Kollmann et al. 2022), show a different pattern both near the outer edge of the A ring and throughout the plot.

Paranicas et al. (2010) originally interpreted the flux decrease on the dayside as the spacecraft moving onto electron drift paths that are forbidden, i.e., intersect the main rings somewhere. In the presence of a noon-to-midnight electric field, the centers of drift circles would shift away from Saturn’s center. In fact, Barbosa & Kivelson (1983; see their Figure 1) illustrated how particle drift orbits would be perturbed, only in a schematic way, if such a field were acting. In reality, the exact shape of the drift orbits, which usually deviate from circular ones, depends on the electron energy and the local time at which the electron is launched (Cooper et al. 1998).

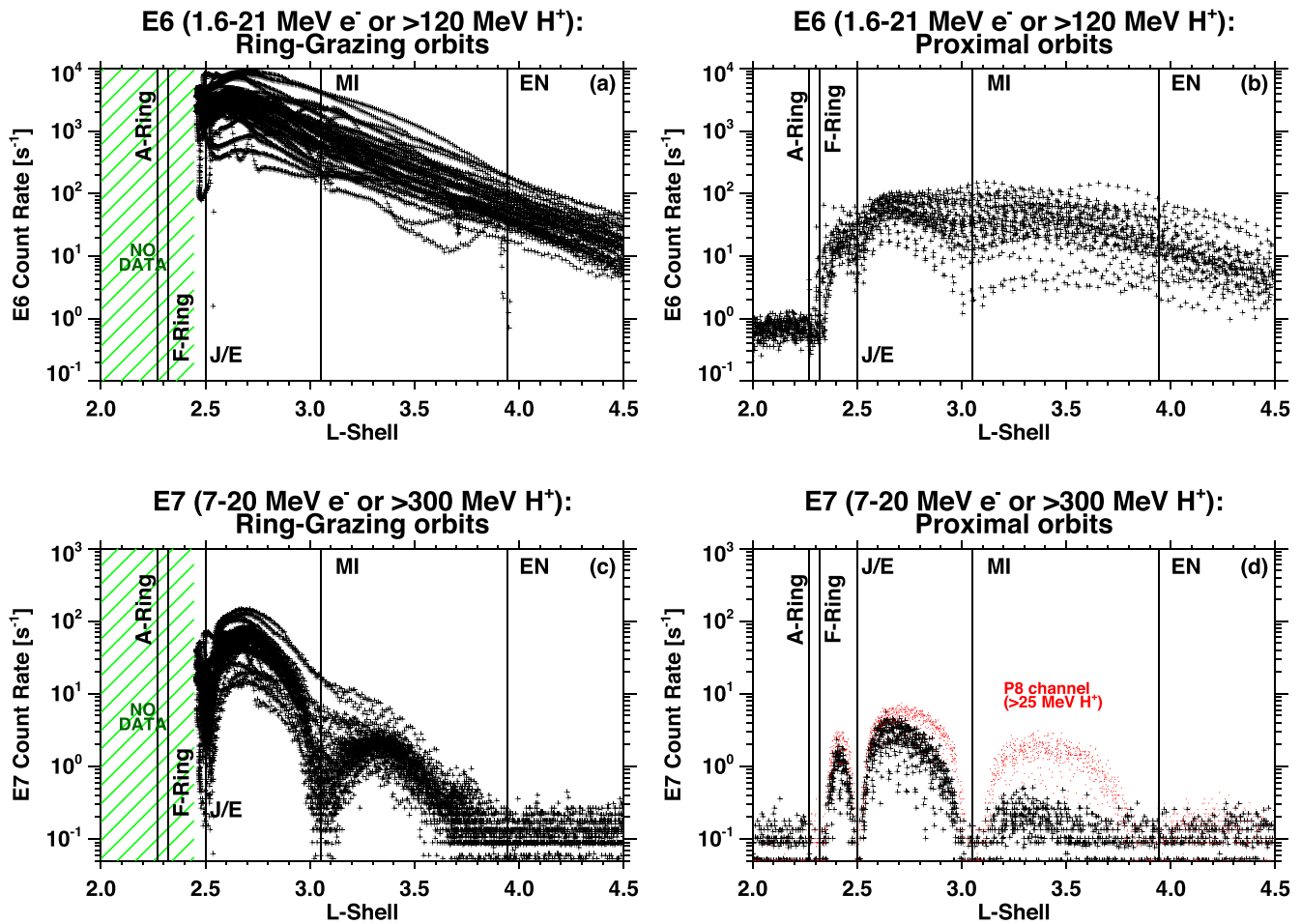


Figure 2. Summary of E6 and E7 count-rate measurements during the Grand Finale orbits. Proton channel P8 is also shown in panel (d). The positions of several key moons and rings are indicated as vertical lines.

Roussos et al. (2019; see their Figure 3) carried out a simulation of equatorial drift paths around Saturn with a realistic value of an electric field magnitude of 0.025 mV m^{-1} and found many prograde electrons launched on the dayside would indeed intersect the main rings.

At Saturn, the cold plasma and most electrons move in the prograde sense. But at a “resonance” energy, electrons have nearly zero net longitudinal motion, i.e., the gradient-curvature drift speed is equal and opposite to the corotation speed. Near the main rings, this resonance occurs at about 4 MeV. Roussos et al. (2007; see Figure 1) have calculated the resonant energy over a range of L shells; above this energy, electrons travel retrograde around Saturn.

Barbosa & Kivelson (1983) showed the equatorial projection of a particle’s guiding center would approximate a circle, but its center would be offset in the direction opposite to a global electric field, i.e., toward -E. This applies to prograde particles and is the basis of the explanation of the dropout near the rings in Paranicas et al. (2010), namely, that the drift circles shifted toward noon. However, for retrograde electrons, the perturbed circle would shift toward +E. Since LEMMS channel E7 nominally measures 7–20 MeV (and therefore retrograde) electrons, their expected drift circles would be shifted toward midnight in this picture. If there were no other factors to consider, we might expect the E7 channel to be populated with flux right up to the A-ring edge on the inbound in Figure 1. Since the E7 fluxes do not reach the ring edge on the inbound,

Thomsen et al. (2012) questioned whether the electric field might not extend inward to the ring edge.

Other issues make the E7 data complicated to interpret. As noted above for P2, LEMMS channels have a nominal energy passband for each species that contributes to the channel foreground. But many channels can also receive counts from other species/energies that are usually measured with very low efficiencies. Furthermore, in an environment where there are very few counts from the nominal species/energies, the channel could be dominated by other species/energies if their flux is high enough. It is possible the E7 rate ($<1 \text{ count s}^{-1}$) outbound very close to the main rings is due to prograde electrons measured at low efficiency, since MeV protons are absent at that location. Finally, on the inbound, while all E channels shown seem to drop in parallel only in the vicinity of the F ring, E7 experiences additional dropouts at other moon locations (Mimas, Janus/Epimetheus, etc). Outbound, E4–E6 have rather flat profiles, whereas E7 still experiences losses at all moon and ring L shells.

3. Grand Finale Orbits

In Figure 2, we show a summary of the LEMMS channels E6 and E7 from the 20 ring-grazing orbits (left-hand side) and the 21 proximal orbits (right-hand side) in Cassini’s Grand Finale orbits. These orbits can offer further insights into the radiation belt dynamics at L shells adjacent to the A-ring edge,

providing increased statistical value to the SOI observations. The electron contribution to these channels would most likely be dominated at the low end of the energy range shown, since electron spectra drop steeply above a few MeV (Sun et al. 2019; Selesnick 1993). The measurements were associated with an L shell by mapping to the magnetic equator following Roussos et al. (2019).

Both types of orbits had periods of about 1 week. Given that and the fact that the two mission orbit segments are sequential (e.g., they belong to the same solar cycle phase), we expect radiation belt variability levels during both the proximal and the ring-grazing orbits to be similar. Any difference in the observed variability conditions between the ring-grazing and the proximal orbits could only be attributed to the geometry of the two orbit types: the ring-grazing orbits reached inward to about $L=2.4$, and sampled mid-to-low magnetic latitudes when crossing the inner radiation belts. Thus, they cannot be used to assess the A-ring absorption of electrons, which occurs farther in. The proximal orbits reached all the way to the planet ($L=1$), and crossed the field lines that map to the A-ring edge and the radiation belts at $L > 2.27$ at very high north or south latitudes ($>50^\circ$).

One complication with the LEMMS electron channels used here near the main rings is as follows. Roussos et al. (2018) showed that inward of the main rings, penetrating radiation was very important for understanding the response of the LEMMS channels. That is, out-of-passband particles can contribute meaningfully to the count rate. For example, Krupp et al. (2018) pointed out that many of the LEMMS channels can receive counts from 60 MeV or greater charged particles. In addition, Roussos et al. (2018) proposed that very energetic protons were present in high numbers in interpreting MIMI data between Saturn and the main rings. The Cosmic Ray Albedo Neutron Decay mechanism can produce energetic protons that can be trapped close to the planet (Cooper 1983).

As noted on Figure 2, channels E6 and E7 are also among the channels that have counts from energetic electrons and protons. While they were originally designed to measure electrons, E6 and E7 may also capture protons of >120 and >300 MeV, respectively. It is even possible for these channels to be dominated by such counts under certain environmental conditions. Preliminary work based on Kollmann et al. (2022) suggests E6 is mainly an electron channel just outward of the main rings whereas E7 may receive as many as half its counts from protons. It is useful then in the discussion of the data that follows to assume E6 is an electron channel with some proton contamination while E7 is a channel with important contributions from both electron and protons.

Most notable among the Figure 2 features for this analysis is the different L-shell profile and scatter of the data depending on the mission phase and the channel considered. The scatter of the data at a given L shell is largely indicative of how variable the radiation belts are, although part of it can be attributed to the different pitch angle sampling by LEMMS during different orbits. The E6 data during the ring-grazing orbits (panel (a)), for example, scatter up to 1 order of magnitude and are above the background at the moon (Enceladus, Mimas, Janus/Epimetheus) and F-ring L shells, two features that can be used to separate electrons from protons (e.g., Roussos et al. 2014). In this radial range, very energetic proton fluxes are typically near background at the moon orbits and quasi-stable elsewhere (e.g., Kollmann et al. 2017). The E7 data during the ring-grazing

orbits (panel (c)) also show considerable variability, and partly filled moon L shells, suggesting that 7–20 MeV electrons do contribute to the channel’s count rate. The low count-rate envelope of the same profile, however, resembles that of protons (panel (d), red points). Finally, E6 (panel (b)) shows responses can occur inward of the F ring, the same as during SOI.

During the proximal orbits, when there were measurements at the edge of the A ring ($L \sim 2.27$, panel (b)), E6 shows that there are times the count rate is above background, whereas E7 (panel (d)) shows a subtle but detectable drop off outward of the A ring, reaching background levels. The weak signal above the rings ($L < 2.27$) originates from electrons directly emitted from the main rings following the Galactic cosmic-ray collisions (Roussos et al. 2019). Further out from the A-ring edge, E6 is variable, like it was during the ring-grazing orbits (panel (a)), but count-rate levels are much lower. This is likely because the access of trapped particles usually drops with increasing latitude. This variability suggests that proximal orbit E6 rates are dominated by electrons. Unlike E6, the E7 data share a similar profile with >25 MeV protons from channel P8 (panel (d), red points). It is especially interesting that E7 electrons do not show the variability seen in the corresponding, lower-latitude, ring-grazing orbits (i.e., compare the level of variability in panels (c) and (d)).

The similarity of the E7 proximal orbit L-shell profile to the proton profile alone, however, may not be sufficient to determine what this channel measures at high latitudes. E7 is clearly a complicated channel and next we will describe other issues with its interpretation near the main rings. Electrons in the nominal E7 energy passband behave more like protons when it comes to interacting with Saturn’s moons. They will, for example, re-encounter the Janus/Epimetheus pair much faster than electrons at lower energies. At $L=2.5$, 1.9 MeV protons and 10 MeV electrons with mirror latitudes of 5° , both take about 5 hr to complete a rotation of Saturn, although they travel in opposite directions. By comparison, 1 MeV electrons with the same mirror latitude and L shell take about 18 hr. This means that E7 electrons can show flux decreases related to absorption by moons and rings that might be absent in lower energy electron data.

In addition, the electric field is most efficient at moving particles radially when they are near the resonance, i.e., move very slowly in local time (Roussos et al. 2018). On the other hand, because of their much faster drift, E7 (>7 MeV) electrons, like MeV protons, are not easily moved radially by the field. That could be another reason that moon L shells in the L-shell profiles of channel E6 are more regularly filled, whereas this happens in E7 less frequently. It may be that the similarities of the E7 and MeV proton channel measurements can still be explained with basic particle drift physics and moon/ring losses, even if E7 is dominated by electrons everywhere. This raises the question, if radial transport episodes are intense enough to occasionally fill the moon corridors (in the L-shell profiles of ultrarelativistic electrons like E7) at low latitudes, why do we not see that happening at high latitudes, during the proximal orbits?

Yuan et al. (2021) found that the same energetic electron measurements discussed here, including the 7–20 MeV ones measured by E7, have butterfly equatorial pitch angle distributions (PADs) outward of the main rings, peaking at an equatorial pitch angle around 55° , whereas proton PADs are

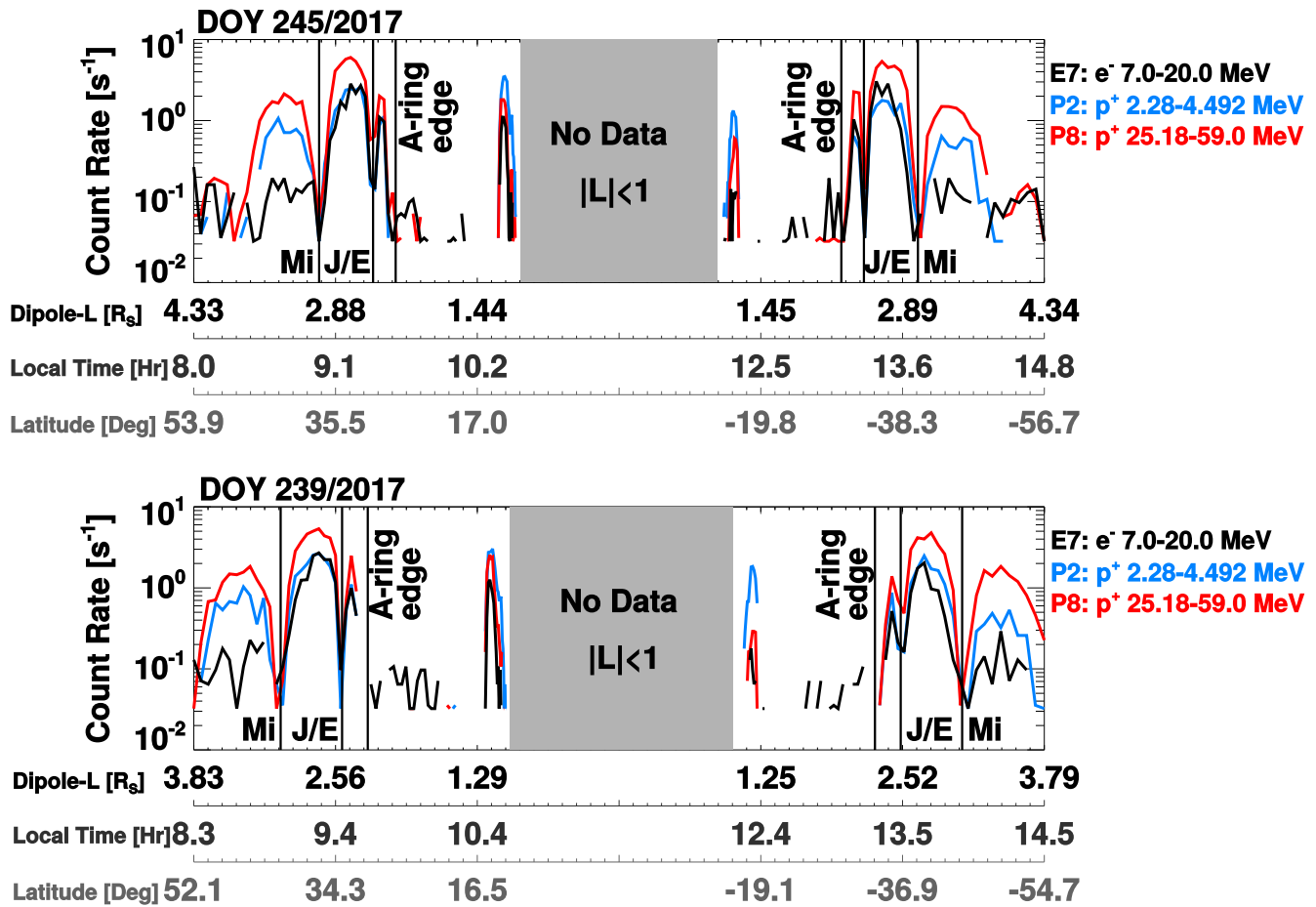


Figure 3. Count rates from E7, P2, and P8 are shown from two dates in 2017 with a mapping to an L shell.

peaked at 90° . They additionally showed that fluxes at equatorial pitch angles of $\sim 15^\circ$, i.e., the maximum value that could be measured at Cassini’s high-latitude proximal orbits in the $L > 2.27$ radiation belts, are more than 20 times below the peak values at $\sim 55^\circ$, indicating that the E7 signal falls rapidly with latitude at those distances. Contrary to that, the pitch angle variability of the MeV proton count rates (Roussos et al. 2011) is lower than a factor of 2. It is thus possible that with increasing latitude, the >300 MeV energetic proton signal in E7 overtakes that of the rapidly diminishing >7 MeV electron count rates, and becomes dominant.

The conclusion above is durable even when we consider individual orbit data, rather than the statistical aggregate. Figure 3 shows a comparison of the count rate from channels E7, P2 (>60 MeV penetrating proton indicator), and P8 from two sample orbits on days 2017-245 and 2017-239. The responses of these channels are similar both in overall shape and sometimes count rate. As noted, the similarity of the E7 shape to P2 and P8 can be due to both the rapid rate at which these particles orbit the planet and also the presence of an unknown level of MeV protons in the count rate. We suggest, based on all these factors, that E7 likely has strong proton contributions outward of the main rings (and this is what preliminary simulations also found) and these may be a larger fraction of the signal at high latitude. In addition to these points disqualifying E7 as a good probe of the electric field near the rings, the short times at which the likely contributors to E7

orbit Saturn mean they are less responsive to the E field in any case.

4. Discussion

Paranicas et al. (2010) proposed that an electric field could explain the abrupt decrease of energetic electron flux observed by Cassini outward of the main rings around noon local time. Energetic electrons are not easily lost to material interactions (like neutral gas or faint dust rings), so the change in flux was notable. Thomsen et al. (2012) raised the objection that a single energy channel in LEMMS was not consistent with this interpretation. On the other hand, Thomsen et al. (2012) also presented evidence from the waves data that supported the idea of an electric field at the ring edge.

But as we argued here, LEMMS channel E7 is not a reliable channel for sensing the electric field near the main rings. E7 electrons have high longitudinal speeds meaning their fluxes in local time are not shaped as much by the electric field and the electrons in the channel have more material interactions. On this latter point, moon and ring absorption is not a source of local time or longitudinal asymmetry for electron channels that cover the low MeV energy range, but it can be a factor for ultrarelativistic electrons. Near the A-ring edge, ultrarelativistic electrons encounter multiple nonuniformly distributed obstacles, for example, the F ring and its clumps, or the asteroid-sized moons shepherding the F ring, Prometheus and Pandora. The effects of these obstacles on channel E7 are clearly present

both inbound and outbound at SOI. This interpretation is also not inconsistent with low fluxes of E7 electrons at high latitudes and near the A ring.

Therefore, we conclude, as we did previously, that the transient electric field at Saturn extends outward from the edge of the main rings through the inner magnetosphere. While this explanation may be eclipsed in the future, the assumption of a global electric field at Saturn is useful practically for explaining many features of the plasma and energetic charged particle data, including the banded features that appear in the flux, observed on many Cassini orbits (Hao et al. 2020). It is important to keep in mind that it is transient in nature: the variable count-rate profiles of E6 and E7, particularly in the ring-grazing orbits, and the transient filling of the moon L shells with electrons (Figures 2(a) and (c)) means that some data, on individual orbits, will not be organized by it. If the electric field fluctuates (e.g., Roussos et al. 2018; Sun et al. 2021), the energetic charged particle distributions near Saturn's main rings are probably not static.

This work was funded under federal award Nos. 80NSSC19K0886 and 80NSSC21K0534, research grants between NASA and The Johns Hopkins University.

Open research. The Planetary Data System provides access to the calibrated LEMMS data at <https://pds-ppi.igpp.ucla.edu/search/view/?id=pds://PPI/CO-S-MIMI-4-LEMMS-CALIB-V1.0>.

ORCID iDs

C. Paranicas  <https://orcid.org/0000-0002-4391-8255>
 E. Roussos  <https://orcid.org/0000-0002-5699-0678>
 K. Dialynas  <https://orcid.org/0000-0002-5231-7929>
 P. Kollmann  <https://orcid.org/0000-0002-4274-9760>
 N. Krupp  <https://orcid.org/0000-0003-4683-9533>

M. Hedman  <https://orcid.org/0000-0002-8592-0812>
 R. C. Allen  <https://orcid.org/0000-0003-2079-5683>
 G. Hospodarsky  <https://orcid.org/0000-0001-9200-9878>

References

- Andriopoulou, M., Roussos, E., Krupp, N., et al. 2014, *Icar*, **229**, 57
 Andriopoulou, M., Roussos, E., Krupp, N., et al. 2012, *Icar*, **220**, 503
 Bagenal, F., & Delamere, P. A. 2011, *JGRA*, **116**, A05209
 Barbosa, D. D., & Kivelson, M. G. 1983, *GeoRL*, **10**, 210
 Cooper, J. F. 1983, *JGR*, **88**, 3945
 Cooper, J. F., Sittler, E. C., Jr., Maurice, S., Mauk, B. H., & Selesnick, R. S. 1998, *AdSpR*, **21**, 1479
 Dialynas, K., Roussos, E., Regoli, L., et al. 2018, *JGRA*, **123**, 8066
 Dialynas, K., Brandt, P. C., Krimigis, S. M., et al. 2013, *JGRA*, **118**, 3027
 Gurnett, D. A., Kurth, W. S., Hospodarsky, G. B., et al. 2005, *Sci*, **307**, 1255
 Hao, Y., Sun, Y., Roussos, E., et al. 2020, *ApJL*, **905**, L10
 Jia, X., & Kivelson, M. G. 2016, *JGRA*, **121**, 1413
 Kollmann, P., Roussos, E., Clark, G., et al. 2022, *Icar*, **376**, 114795
 Kollmann, P., Roussos, E., Kotova, A., Paranicas, C., & Krupp, N. 2017, *NatAs*, **1**, 872
 Krupp, N., Roussos, E., Kollmann, P., et al. 2018, *GeoRL*, **45**, 10847
 Paranicas, C., Mitchell, D. G., Krimigis, S. M., et al. 2010, *JGRA*, **115**, A07216
 Roussos, E., Kollmann, P., Krupp, N., et al. 2019, *GeoRL*, **46**, 3590
 Roussos, E., Kollmann, P., Krupp, N., et al. 2018, *Sci*, **362**, aat1962
 Roussos, E., Krupp, N., Paranicas, C., et al. 2014, *P&SS*, **104**, 3
 Roussos, E., Krupp, N., Paranicas, C. P., et al. 2010, *JGRA*, **115**, A03202
 Roussos, E., Krupp, N., Paranicas, C. P., et al. 2011, *JGRA*, **116**, A02217
 Roussos, E., Jones, G. H., Krupp, N., et al. 2007, *JGRA*, **112**, A06214
 Roussos, E., Krupp, N., Woch, J., et al. 2005, *GeoRL*, **32**, L24107
 Selesnick, R. S. 1993, *AdSpR*, **13**, 221
 Sun, Y. X., Roussos, E., Hao, Y. X., et al. 2021, *JGRA*, **126**, e29600
 Sun, Y. X., Roussos, E., Krupp, N., et al. 2019, *GeoRL*, **46**, 10240
 Thomsen, M. F., Roussos, E., Andriopoulou, M., et al. 2012, *JGRA*, **117**, A09208
 Went, D. R., Hospodarsky, G. B., Masters, A., et al. 2011, *JGRA*, **116**, A07202
 Wilson, R. J., Bagenal, F., Delamere, P. A., et al. 2013, *JGRA*, **118**, 2122
 Yuan, C.-J., Roussos, E., Wei, Y., et al. 2021, *GeoRL*, **48**, e2021GL092690
 Yuan, C.-J., Roussos, E., Wei, Y., & Krupp, N. 2020, *JGRA*, **125**, e27621